SUPPLEMENT SERIES

Astron. Astrophys. Suppl. Ser. **124,** 283-289 (1997)

Spectroscopic and photometric study of the bright X-ray cluster A1300⋆

M. Pierre[1], J. Oukbir[1], D. Dubreuil[1], G. Soucail[2], J.-L. Sauvageot[1], and Y. Mellier[2,3]

[1] CEA Saclay DSM/DAPNIA, Service d'Astrophysique, F-91191 Gif sur Yvette, France
[2] Observatoire Midi-Pyrénées, Laboratoire d'Astrophysique de Toulouse, UMR 5572, 14 Avenue E. Belin, F-31400 Toulouse, France
[3] Institut d'Astrophysique, 98bis Bd. Arago, F-75014 Paris, France

Received July 22; accepted November 6, 1996

Abstract. We present the first results of an optical follow-up of X-ray bright clusters of galaxies located between $0.15 \leq z \leq 0.31$: B and R photometry as well as medium resolution spectroscopy of the galaxies. The cluster studied here - A1300 - is found to have a redshift of 0.3072 and a velocity dispersion of 1210 km/s, based on 52 cluster members. Structures are observed in the galaxy number counts but the velocity histogramme shows no significant departure from a Gaussian distribution[1].

Key words: galaxies: clusters: individual: Abell 1300 — X-rays: galaxies — galaxies: redshifts

1. Introduction

Young rich clusters have very important cosmological implications since they are supposed to originate from the rare initial density fluctuations of high amplitude. In this general context, we have initiated a high resolution multi-wavelength campaign (IR, radio, optical, X-ray) in order to study in detail the properties of distant bright X-ray clusters newly discovered in the ROSAT All-Sky-Survey (RASS), especially in order to better understand their dynamical state (Pierre et al. 1994a). We have selected a set of $\sim$ 10 clusters, having X-ray luminosities greater than 10^{44} erg/s and thus expected to be massive. This implies a high density for the intra-cluster gas and most likely, a deep gravitational potential. The objects are located in the southern hemisphere between $10h \leq RA \leq 14h$ within an area covering some 1700 square degrees. The redshifts cover the range $z = 0.15 - 0.31$, which is ideal for mapping the whole cluster extent within reasonable exposure times. It will also be possible to tackle question related to cluster evolution by comparison with lower redshift observations. The cluster of galaxies A1300 is one of the priority target of the programme and we present here the first results of the detailed optical follow-up concerning this object.

A1300 is described as a richness class 1 object by Abell et al. (1989) and had not drawn specific attention from the community so far. It was observed for the first time in X-ray during the RASS and notified as such during a subsequent identification campaign at the ESO 3.6 m Telescope (Pierre et al. 1994b). These optical observations have shown that the cluster is quite rich, very extended, has a redshift of $\sim$ 0.306 and suggested a high velocity dispersion. The RASS X-ray image is clearly extended, approximately in the SN direction (Pierre et al. 1994b). Preliminary analysis of a subsequent deep PSPC ROSAT pointing shows a distinct clump at the northern end, some $3'$ from the cluster center, corresponding to a conspicuous enhancement of the galaxy density. The X-ray luminosity appeared to be high, $\sim 10^{45}$ erg/s in the ROSAT band, and hard. All of this indicate that A1300 is quite an interesting object - probably exceptional -, one of the few $z \geq 0.3$ clusters having a high X-ray luminosity.

Throughout the paper we assume a Hubble constant of 50 km/s/Mpc and $q_0 = 1/2$.

2. Observations

Four bright X-ray distant clusters detected in the RASS - including A1300 - have been observed during a 4 night run at the 3.6 m CFH Telescope in May 1993. For A1300, medium deep images were obtained in the B and R bands as well as 3 spectroscopic masks, each containing about 30 slits; two of them were centered on the main cluster

Send offprint requests to: M. Pierre
mpierre@ariane.saclay.cea.fr

⋆ Based on observations collected at the Canada-France-Hawaii Telescope at Mauna Kea, Hawaii, U.S.A.

[1] Table 3 (4) is only (also) available in electronic form at the CDS via anonymous ftp to cdsarc.u-strasbg.fr (130.79.128.5) or via http://cdsweb.u-strasbg.fr/Abstract.html

Table 1. Observation summary, cD center (J2000): 11h 31m 54.1s, -19d55′40″

	$10' \times 10'$ field center	Time (min)
Photometry		
R images	cD	15, 10
B images	cD	2×25
Spectroscopy		
1st mask	cD	45, 40
2nd mask	cD	75, 50
3rd mask	3′ north of the cD	60, 75

body and the third one on the northern X-ray sub-clump. Observations are summarized in Table 1.

The focal reducer MOS/SIS together with CCD Lick2 (2048×2048 pixels of 15 μm) were used during the run. This CCD is a thick device having a quantum efficiency of $\sim 10\%$ in the blue. The observing configuration provides a pixel size of 0.314″ over a field of view of about $10' \times 10'$. The overall image quality was good (stellar FWHM $\sim 0.9''$) although some optical distortions were conspicuous near the edges of the images due to the optics of the focal reducer. A control problem in the reading of the CCD, namely the random addition of null pixel values, was unfortunately discovered after the A1300 observations. The resulting main effect on the data is to mimic a misalignement between the grism and the CCD columns such that the dispersion direction appears tilted with respect to the CCD columns whereas the image of the slits remain perfectly aligned along the rows; this can be easily corrected, however, the final spectroscopic resolution in somewhat altered.

3. Photometry

Detailed inspection of images showed that the cluster central galaxy, a cD, has a double nucleus (Fig. 1) but did not reveal any gravitationally lensed feature, despite the large cluster X-ray luminosity. The B and R frames were prepared using standard pre-reduction techniques and in order to avoid strong vignetting effects, only the $7.1' \times 6.5'$ inner field was processed. The photometric analysis was performed by means of the SExtractor package (Bertin & Arnouts 1996): for the R frame (and B, respectively), images are first slightly smoothed by a 1 (1.2) pixel σ Gaussian (comparable to that of the seeing), then the background is estimated using a 64×64 pixel mesh. Sources are detected at a 3 (1.2) σ level above the local background if having at least 5 pixels at this threshold (B exposures are significantly less deep than the R ones, because of the low CCD efficiency in the blue range). Multiple images are automatically deblended by a multithresholding algorithm and each individual object is finally attributed a "class", a number ranging from 0

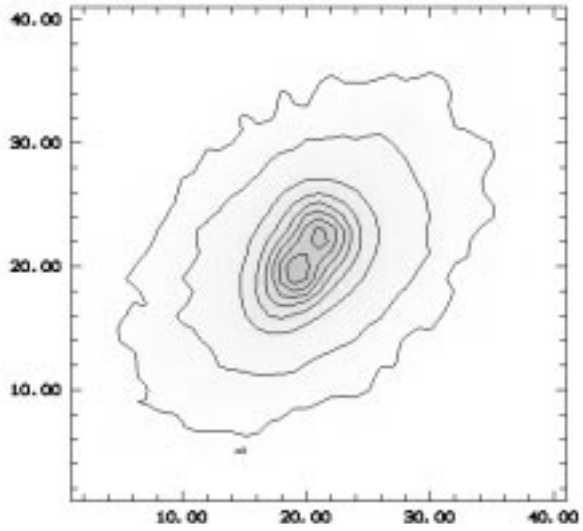

Fig. 1. CFHT R image of A1300 central galaxy revealing a double nucleus. Pixelsize: 0.314″

(galaxy) to 1 (star) by mean of a morphological analysis based on a neuron network. The SExtractor neuron network is of supervised type, the training being done with images containing both stars and galaxies (the input parameters are 8 isophotal areas, the central peak instensity and the seeing). Adaptative aperture magnitudes are computed (inspired from Kron's first moment method); this allows the measurement up to 94% of the object flux over the almost entire magnitude range. For multiple objects, corrected isophotal magnitudes are used which requires conservation of the total flux for the blend. Since only two frames were available in each colour and that we do not search for very faint objects, each frame was processed individually and magnitudes were averaged at the end of the procedure, providing at the same time estimates for the internal measurement errors in each colour (Tables 2 & 3).

Table 2. Standard deviation of magnitude differences measured between two frames. In order to estimate errors for objects listed in Table 3, following values have to be divided by $\sqrt{2}$

$R \leq 20$	0.02	$B \leq 22$	0.06
$20 \leq R \leq 20.5$	0.03	$22 \leq B \leq 22.75$	0.11
$20.5 \leq R \leq 21.5$	0.06	$22.75 \leq B \leq 23.5$	0.14
$21.5 \leq R$	0.07	$23.5 \leq B$	0.20

The final photometric calibrations were done using the CCD Sequence in M 92 (Christian et al. 1995) also observed during the same run; for this purpose, stars VCS1, A, B (probably variable) had to be removed

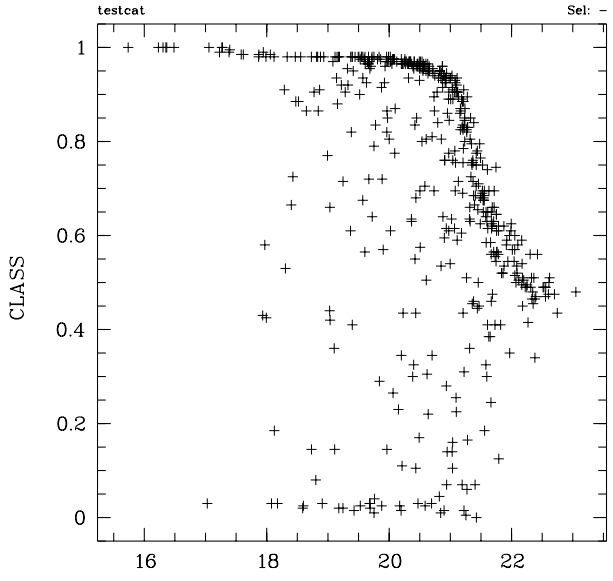

Fig. 2. Galaxy/star separation as a function of R magnitude. Galaxies can be unambiguously identified up to $R \sim 21$. (class ≤ 0.98)

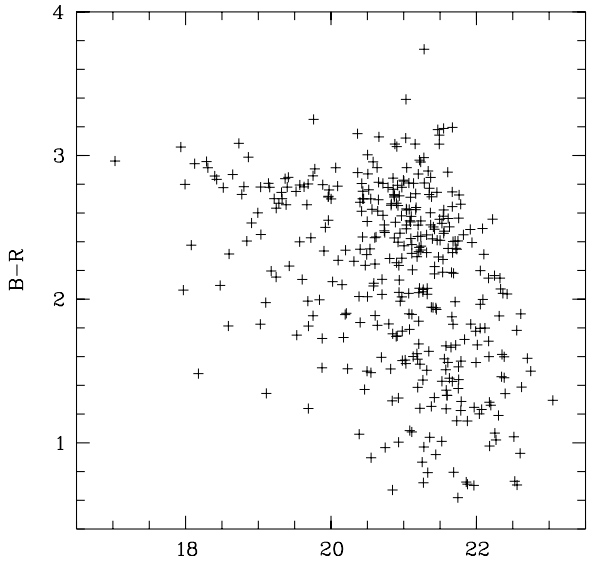

Fig. 3. Colour-magnitude diagramme for objects classified as galaxies

because of obvious inconsistancies. The fraction of galactic stars included in the catalogue was estimated by Robin's model (1995). Between $17 \leq R \leq 21$, 49 stars are expected and this allows us to assume that detected objects having a class up to 0.98 may be considered as galaxies within this magnitude range (Fig. 2).

Consequently, only objects having a R class ≤ 0.98 and detected in all B and R frames are finally retained as galaxies. The rigde observed at the faint magnitude end is a normal feature of the method (cf. Bertin & Arnouts 1996): it corresponds to the degeneracy of the stellar index to intermediate values as magnitude increases. The fact that it is slightly more prononced here comes from small focus variations across the MOS field of view. Whether faint misclassified stars may still be contained in the final catalogue should not be a problem, at least for the shape of the galaxy luminosity and galaxy number density contours, displayed in Figs. 4 and 5 respectively.

Table 3. Photometric analysis of A1300 (beginning; the complete table is available in electronic form at CDS)

x	y	m_R	$B-R$	Class$_R$
−701.8	524.6	19.08	2.00	0.97
−701.3	508.2	21.42	1.31	0.71
−697.6	326.5	19.38	2.66	0.82

Columns 1 & 2: x, y distance from the field center (cD) in pixel unit ($0.314''$).
Column 3: R magnitude (average between 2 frames)
Column 4: $B-R$ colour (average between 4 frames)
Column 5: morphological class in the R band (see text).

The complete object catalogue is presented in Table 3 and photometric errors given in Table 2. Completness limits are $B = 23$ and $R = 21$, which corresponds to 180 galaxies. The total catalogue of Table 3 comprises 480 objects, out of these 431 are classified as galaxies.

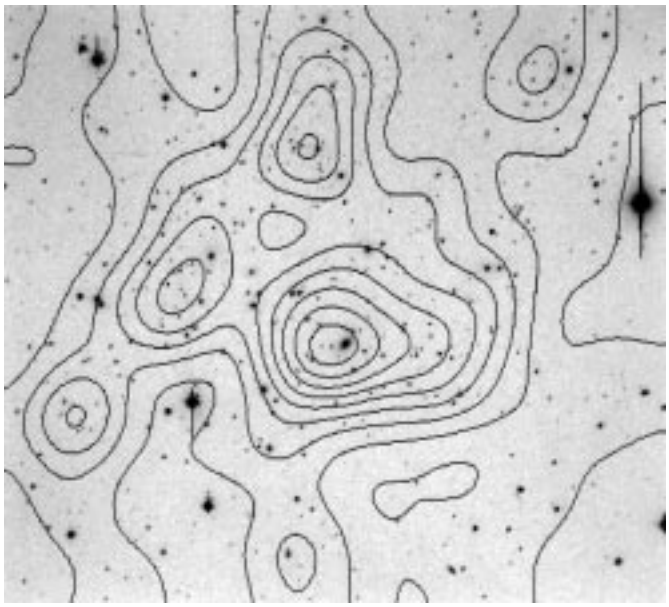

Fig. 4. Galaxy number counts including all galaxies of Table 3. The filtering function has a FWHM of $55''$. The contour increment is ~ 4.5 galaxies/arcmin^2 (image size $7.14' \times 6.54'$)

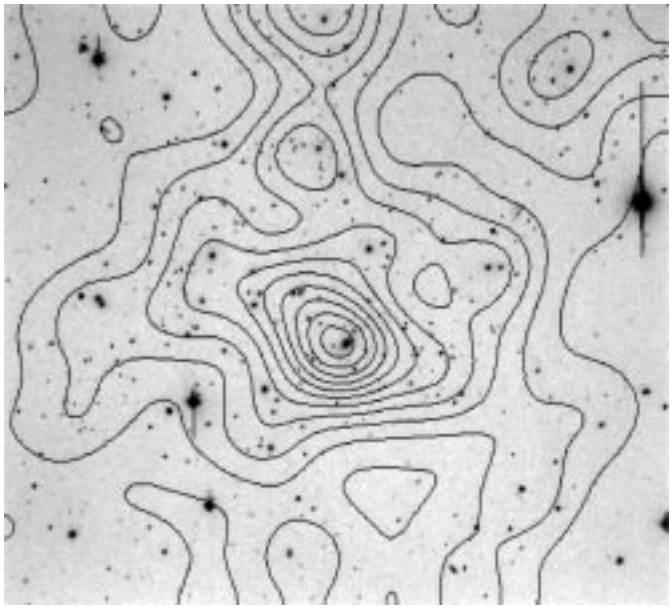

Fig. 5. Galaxy luminosity density coutours including all galaxies of Table 3. The filtering function has a FWHM of 55″. Contour increment is constant in flux. First and last contours correspond respectively to 31.8 and 26.0 m_R/arcmin^2 (image size $7.14' \times 6.54'$)

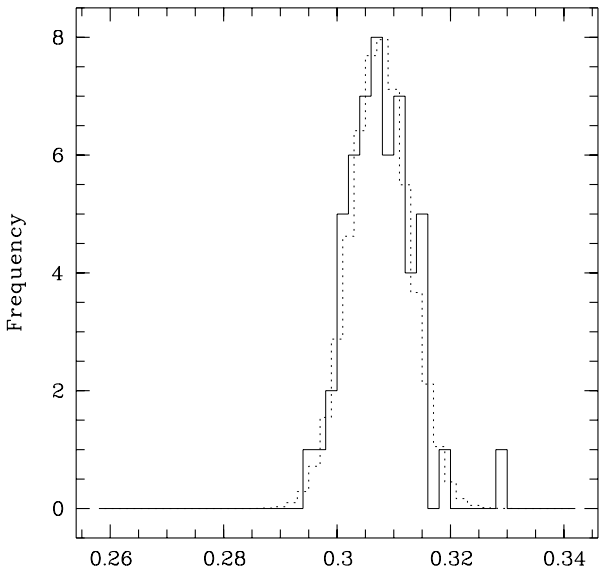

Fig. 6. Cluster galaxy redshift histogramme (binsize: $\delta z = 0.002$); the mean redshift is 0.3072 and the velocity dispersion 1580 km/s. The dotted line represents the best Gaussian fit

4. Spectroscopy

In spectroscopic mode the grism O300 was used. It has a zero deviation at 5900 Å, covers approximately 4700 − 7900 Å and in the MOS configuration presents a dispersion of 3.59 Å/pixel (0.314″). The slit had a width of 2″, i.e. 6.4 pixels, yielding a resolution of ~ 23 Å and slightly oversampled spectra which allowed rebinning along the dispersion direction while CCD reading. Typical line features are spread over more than 3 pixels which for bright spectra enables a redshift accuracy of 150 km/s and of the order of 300 km/s for the faintest objects. Wavelength calibrations were done using internal He+Ar lamps and after standard reductions (including geometrical rectification of the spectra, see Sect. 1). Redshifts were measured by a cross-correlation method following Tonry & Davis (1979) and implemented in the MIDAS environment. Errors were estimated as a function of the correlation parameter r: $\delta z = k/(1 + r)$, where k has been determined for the present observing configuration by noise degradation of high S/N spectra ($k = 0.0029$). The results from the cross-correlation analysis for faint spectra were in turn checked by hand and the presence of a few conspicuous absorption lines was required, for them to be included in the final list which is presented in Table 4. (Correction for heliocentric motion is ≤ -20 km/s, and thus totally negligible). Finding charts for the measured galaxies can be found in Figs. 7 and 8.

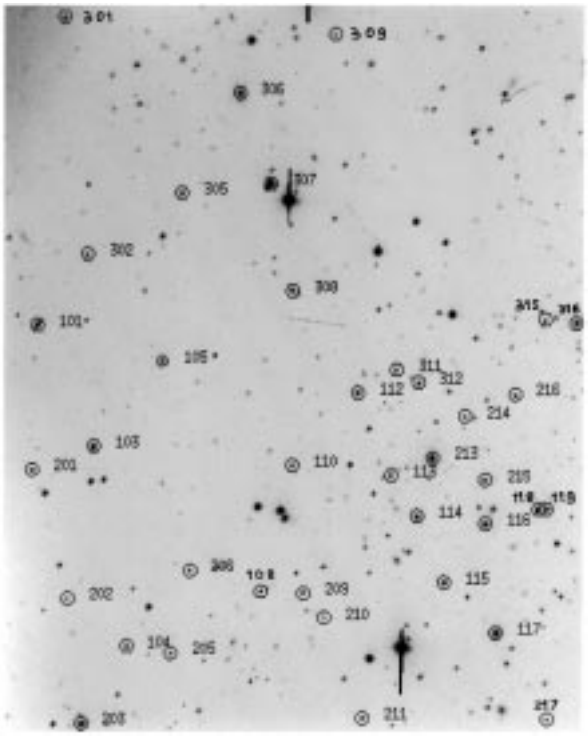

Fig. 7. Finding chart for galaxies with measured redshifts: EAST (image size $4.72' \times 6.02'$)

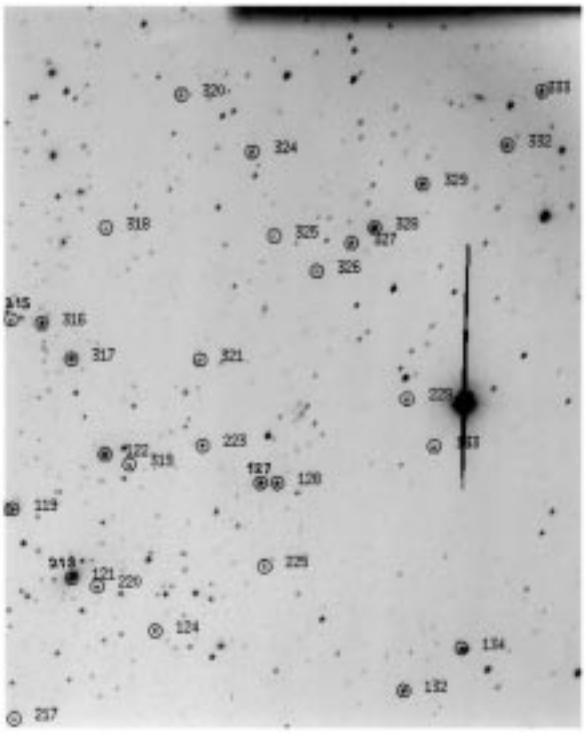

Fig. 8. Finding chart for galaxies with measured redshifts: WEST (image size $4.72' \times 6.02'$)

Cluster membership was assessed using a 3σ clipping method and 52 galaxies were found to belong to the cluster. Corresponding cluster galaxy redshift histogram is presented in Fig. 6. It is very broad but does not show significant sub-structure. It is well fitted by a Gaussian centered on $z = 0.3072$ and a $\sigma_{\rm v}$ of 1580 km/s, which corroborates well the results by Pierre et al. (1994b) obtained only with 8 galaxies observed at the ESO 3.6 m Telescope. If only the 47 galaxies with spectra of quality 1 and 2 are included (see caption of Table 4) similar values are obtained (0.3073, 1580 km/s). Applying the redshift correction, we finaly find an intrinsic velocity dispersion of 1210 km/s. Following Danese et al. (1980) we can estimate the 68% confidence error on these parameters: $\delta z = \pm 0.0007$, $\delta\sigma_{\rm v} = \pm^{380}_{260}$ km/s. Within these uncertainties the cD galaxy ($z = 0.3077$) can be considered to be at rest with the mean cluster velocity. The observed velocity dispersion is large and hard to reconcile with the picture of a single well relaxed cluster.

The velocity data was investigated in more detail using the ROSTAT package (Beers et al. 1990). As shown by Bird & Beers (1993), the skewness and kurtosis are very sensitive in testing the Gaussian hypothesis of the data distribution. In our case – and after removal of the non–cluster galaxies with the 3σ clipping method – we find that the skewness $B1$ is equal to -0.006 and that the kurtosis $B2$ is equal to 2.512. These results mean that the velocity distribution has a tail which slightly extends out towards more negative velocity and that it is more peaked than a normal distribution. However, the significance levels for $B1$ and $B2$ are 0.493 and 0.275 respectively and none of them constitutes a significant rejection of the Gaussian hypothesis. This is illustrated in Fig. 6, where a Gaussian with characteristics similar to that of the observed velocity distribution is superimposed on the data points: the visual impression supports the above results of probably relaxed velocity data. The adopted binsize for the histogramme is 600 km/s (to minimize statistical fluctuations) therefore, any structure in the velocity distribution should be investigated below this value and would require to measure at least twice as many galaxies as well as to use a higher spectral resolution.

5. Conclusions

With a velocity dispersion of the order of 1200 km/s, the cluster of galaxies A1300 is certainly peculiar and the present study reinforces the need to follow-up this object in greater detail. Matter and light distributions as revealed by Figs. 4 and 5 show a significant signal in the vicinity of the cD, and exactly centered on the cD as it would normally be expected at least for the luminosity distribution. In contrary to several clusters (Allen et al. 1995), no overall alignment with the cD main axis is conspicuous, but the number density contours seem to indicate the presence of several sub-groups of galaxies especially East and North of the cluster center, the latter having an X-ray counterpart as already mentioned in Sect. 1. This, all together suggests that the cluster could have undergone a merging at some stage. This hypothesis will be investigated in detail in a comprehensive forthcoming paper combining high resolution deep X-ray and radio observations with the present optical study (Lemonon et al. 1997).

Acknowledgements. It is a pleasure to thank E. Bertin and S. Arnouts for many helpful discussions about the photometric package SExtractor. We acknowledge support from the "GdR Cosmologie".

References

Abell G.O., Corwin H.G., Olowin O.P., 1989, ApJS 70, 1
Allen S.W., Fabian A.C., Edge A.C., Böhringer H., White D.A, MNRAS 275, 741
Beers T.C., Flynn K., Gebhardt K., 1990, AJ 100, 32
Bertin E., Arnouts S., 1996, A&AS 117, 393
Bird C.M., Beers T.C., 1993, AJ 105, 1596
Christian C.A., Adams M., Barnes J.V., Buchter H., Hayes D.S., Mould J.R., Siegel M., 1985, PASP 97, 363
Danese L., De Zotti G., di Tullio G., 1980, A&A 82, 322
Pierre M., Hunstead R., Reid A., et al., 1994a, ESO Messenger December 1994; Multi-wavelength study of ROSAT clusters of galaxies
Pierre M., Böhringer H., Ebeling H., Voges W., Schuecker P., Cruddace R., MacGillivray H., 1994b, A&A 290, 725
Robin A., 1995,"http: //WWW.obs-besancon.fr/www/modele/modele.html"
Tonry J., Davis M., 1979, AJ 84, 1511

Table 4. Spectroscopic analysis of A1300 (also available in electronic form at CDS)

ID	RA_{2000}	Dec_{2000}	z	$\delta\ z$	Q	R	$B-R$	member
101⋆	173.0569	−19.8929	0.1954	0.0008	9			N
103⋆	173.0488	−19.9095	0.1963	0.0013	9			N
104	173.0440	−19.9371	0.3041	0.0009	1			Y
105	173.0390	−19.8978	0.3150	0.0005	1	19.17	2.98	Y
108	173.0248	−19.9295	0.2256	0.0001	9	19.67	2.07	N
110	173.0203	−19.9122	0.3032	0.0009	2	19.67	1.08	Y
112	173.0109	−19.9022	0.3067	0.0006	1	19.14	2.81	Y
113	173.0061	−19.9136	0.3017	0.0008	1	19.49	2.68	Y
114	173.0024	−19.9192	0.3033	0.0004	1	18.77	2.73	Y
115⋆	172.9985	−19.9283	0.3044	0.0011	1	19.10	1.98	Y
116	172.9926	−19.9202	0.3193	0.0009	1	18.52	2.78	Y
117	172.9911	−19.9353	0.3137	0.0004	1	18.08	2.38	Y
118	172.9850	−19.9183	0.1506	0.0006	1	18.47	2.09	N
119	172.9839	−19.9183	0.3032	0.0007	1	18.73	3.08	Y
121	172.9754	−19.9278	0.3077	0.0007	1	17.03	2.96	Y
122	172.9706	−19.9108	0.3159	0.0008	1	18.12	2.94	Y
124	172.9634	−19.9352	0.3002	0.0009	1	19.65	2.59	Y
127	172.9483	−19.9148	0.3014	0.0007	1	18.29	2.96	Y
128	172.9459	−19.9148	0.3027	0.0007	1	18.86	2.99	Y
132	172.9278	−19.9436	0.3044	0.0008	1	18.65	2.87	Y
133	172.9233	−19.9099	0.3150	0.0010	1	19.84	1.99	Y
134	172.9194	−19.9378	0.3076	0.0014	9			Y
201	173.0576	−19.9128	0.3146	0.0007	1			Y
202	173.0525	−19.9305	0.3048	0.0011	2			Y
203	173.0504	−19.9477	0.3063	0.0005	1			Y
205⋆	173.0377	−19.9380	0.3121	0.0011	1	20.02	2.12	Y
206	173.0349	−19.9266	0.3087	0.0009	1	19.92	2.50	Y
209	173.0187	−19.9298	0.3045	0.0007	1	19.60	2.77	Y
210	173.0157	−19.9331	0.3101	0.0012	2			Y
211	173.0102	−19.9470	0.2947	0.0010	2	19.60	2.14	Y
213	173.0002	−19.9112	0.3016	0.0009	9	18.03	2.85	Y
214	172.9956	−19.9054	0.3109	0.0009	1	20.02	2.79	Y
215	172.9926	−19.9142	0.3115	0.0010	9	19.03	2.45	Y
216	172.9884	−19.9024	0.3121	0.0008	9	19.55	2.43	Y
217	172.9837	−19.9472	0.3137	0.0008	1	20.00	2.70	Y
219	172.9753	−19.9277	0.3077	0.0007	2			Y
220	172.9717	−19.9289	0.3021	0.0009	1	19.53	2.79	Y
223	172.9566	−19.9096	0.3018	0.0008	1	19.32	2.74	Y
225⋆	172.9477	−19.9263	0.3031	0.0009	1	20.08	2.73	Y
229	172.9272	−19.9033	0.2989	0.0010	1	19.63	2.78	Y
301	173.0530	−19.8504	0.3598	0.0012	2			N
302	173.0497	−19.8830	0.0588	0.0010	2			N
305	173.0362	−19.8746	0.3098	0.0007	1	19.08	1.99	Y
306	173.0279	−19.8609	0.3115	0.0010	1			Y
307	173.0235	−19.8734	0.2063	0.0010	1			N
308	173.0203	−19.8881	0.3044	0.0009	1	19.16	2.78	Y
309	173.0142	−19.8529	0.3108	0.0009	1			Y
311	173.0054	−19.8990	0.3040	0.0010	1	19.70	2.68	Y
312	173.0022	−19.9008	0.3437	0.0013	2	19.33	2.70	N
315	172.9841	−19.8922	0.3108	0.0006	1	19.66	2.49	Y
316	172.9797	−19.8927	0.3082	0.0006	1	18.40	2.86	Y
317	172.9754	−19.8976	0.3076	0.0008	1	18.43	2.83	Y
318	172.9704	−19.8795	0.3108	0.0011	1			Y

Table 4. continued

ID	RA_{2000}	Dec_{2000}	z	$\delta\ z$	Q	R	$B-R$	member
319	172.9671	−19.9122	0.3099	0.0010	9	19.55	2.81	Y
320*	172.9595	−19.8613	0.2999	0.0013	2			Y
321*	172.9570	−19.8978	0.2980	0.0013	9	19.42	2.23	Y
324	172.9494	−19.8692	0.3082	0.0006	1	19.25	2.63	Y
325	172.9462	−19.8808	0.3150	0.0012	2			Y
326	172.9401	−19.8857	0.3283	0.0009	9			N
327	172.9352	−19.8818	0.2571	0.0009	1	19.22	2.70	N
328	172.9318	−19.8797	0.2575	0.0007	1	17.99	2.80	N
329	172.9250	−19.8737	0.2569	0.0008	1	18.80	2.78	N
332	172.9128	−19.8685	0.3100	0.0010	2			Y
333	172.9078	−19.8611	0.3079	0.0009	1			Y

Column 1: internal number refering to Figs. 7, 8.
Columns 2 & 3: RA and Dec (J2000), decimal degrees. Galaxy positions were interactively measured on the STScI digitized blue sky survey images having a pixel size of $1.7''$, and should have an accuracy of $\sim 3.4''$.
Column 4: redshift.
Column 5: error on the redshift.
Column 6: z measurement quality (1: highest peak in the correlation function, 2: 2nd peak, 9: interactive measurement with lines).
Column 7: R magnitude (only for galaxies within the area processed for photometry).
Column 8: $B-R$ index.
Column 9: cluster member galaxy (3σ clipping method).
Presence of emission lines (*):
101: H_α.
103: H_α.
115: [OII] at 3727, H_β, [OIII] at 4959 and 5007, OI at 6300 and 6364, H_α, NII at 6549 and 6583, SII at 6717 and 6734.
205: H_α, H_β?
225: OI at 6300 and 6364.
320: H_α?
321: H_α? SII at 6717.

The two nuclei of the cD galaxy correspond to numbers 121 & 219 and show totally similar redshifts at the present spectrocsopic resolution.